In silico screening of pyridine coordination and thermodynamic stability in zinc–pincer complexes

Sharol Madera
s3691977 - 5894298

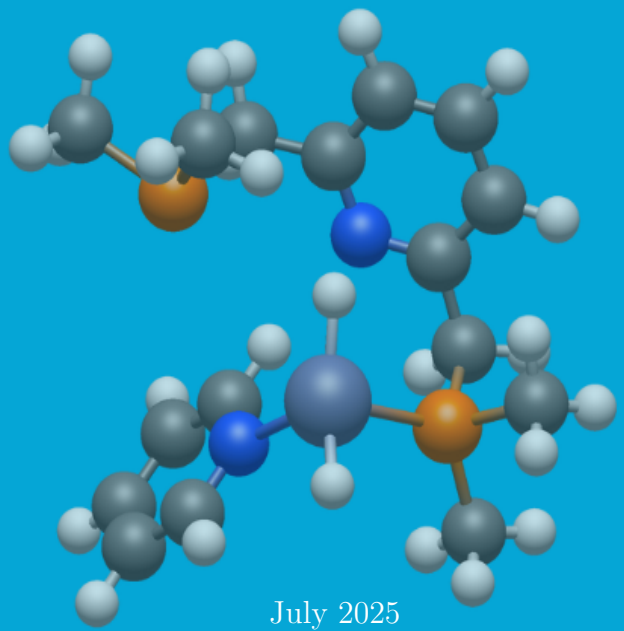

July 2025

TU Delft

In silico screening of pyridine coordination and thermodynamic stability in zinc–pincer complexes

by

Sharol Madera

to obtain the degree of Bachelor of Science
at the Delft University of Technology,
to be defended publicly on Tuesday July 22, 2025.

Performed at:
Inorganic Systems Engineering
Chemical Engineering
Faculty of Applied Sciences

Under supervision of:
Prof. Dr. E. A. Pidko
PhD candidate A. Kalikadien
Dr. A. Kolganov

Student number:	5894298/s3691977
Project duration:	April 23, 2025 – July 22, 2025
Thesis committee:	Prof. Dr. E. A. Pidko, Dr. T. Bouwens, Dr A. Kolganov & Mr. Kalikadien

ABSTRACT

This study is an *in silico* screening of zinc PNP and NNN pincer complexes with variation of the R groups in the ligands for the homogeneous catalysis of the hydrogenation of pyridine. This was done by investigating geometry, hemilability, and binding energies. The scope lies in identifying which complexes are thermodynamically capable of binding pyridine, which is researched using the Gibbs free energy of the binding reaction. Energies and optimized geometries were obtained using Density Functional Theory with ORCA and the supercomputer Snellius. The screening revealed that PNP-R complexes favor tetrahedral geometries after optimization, but three and five coordinated structures are also possible. Hemilability of the phosphorus and/or nitrogen arm were observed. All PNP-complexes showed thermodynamically unfavored binding of pyridine. Additionally, NNN-R complexes did not bind to pyridine. Only when phenyl was used as the R group in the NNN backbone did pyridine bind. This is believed to be due to a hydride migrating to one of the phenyl rings, but even then, the binding energy was not thermodynamically favorable. Moreover, research on ligand substitution by pyridine showed that in most complexes this reaction is unfavorable. Only in three coordinated structures of NNN was this reaction thermodynamically feasible. These findings contribute to understanding the pincer ligand dynamics of PNP and NNN complexes and suggest directions for future research.

Contents

1 INTRODUCTION

1.1 Theoretical Background

As the population grew more & more in the early 20^{th} century, the demand for crops grew simultaneously [1]. In 1913 [2], Fritz Haber developed a method to produce ammonia, an artificial fertilizer, from a chemical reaction of nitrogen and hydrogen at high temperatures [3]. This reaction, called *Ammonia Synthesis*, uses iron as a catalyst, which helps lower the activation energy by allowing nitrogen and hydrogen atoms to stick to its surface, dissociate, and recombine to form ammonia [4]. Catalysts not only reduce the energy barrier of a reaction but also improve selectivity, increase reaction rates, and accelerate chemical reactions [5]. In general catalysts can be split into two groups, which are homogenous and heterogeneous catalysts. Homogeneous catalysts are in the same phase as their reactants, whereas heterogeneous catalysts are in different phases [6]. Modern chemical industry relies heavily on catalysis. Petrochemical, pharmaceutical, and energy industries use catalysts to facilitate the production of products like fuels, fertilizers and polymers [7].

As global challenges evolve, one of the main problems in the 21^{st} century is global warming, driven in part by carbon dioxide emissions from the use of fossil fuels for energy. Therefore, the transition towards sustainable energy is crucial. In the last decade there has been research on finding a new source for energy storage. Alternative energy carriers like hydrogen have been investigated and used but have not entirely subtituted fossil fuels. Reasons for this are the complexity, cost and safety concerns of hydrogen storage [8]. Current methods used for hydrogen storage are for example compressed gas, liquid hydrogen, cold compressed and hydride complexes [9].

Hydrogen storage has become an active area of research with a focus on material based methods like hydrogenation reactions. Hydrogenation is a reaction in which a hydrogen molecule adds to an unsaturated bond. Therefore, the molecule with the unsaturated bond 'stores' the hydrogen [10]. One hydrogen storage option that is increasing expectations is that of liquid organic hydrogen carriers (LOHCs), which are organic compounds that remain in the liquid phase around ambient conditions and can store and release hydrogen by reversible (de)hydrogenation [11]. One of the most studied LOHCs are toluene and methylcyclohexane, which uses transition metals catalysts like platinum, palladium and ruthenium [11]. Other LOHCs of interest are those based on N-heterocycles, such as 1-methyl-octahydroindole, tetradecahydrophenazine, and one of the simplest examples, pyridine. [12]. N-heterocycle hydrogen carriers have low hydrogen extraction temperature compared to other LOHCs due to their low enthalpy of dehydrogenation reaction, which means that less energy is required for this reaction to occur [13]. This contributes to a more energy efficient system and supports the transition to sustainable energy.

Suitable catalytic systems such as metal-ligand complexes are required for the use of LOHCs. These complexes are of great importance in hydrogenation processes due to their structural stability and reactivity. One promising catalytic application is that of pincer-metal complexes. These ligands are tridentate ligands which bind with the metal central atom and form a pincer-like structure, like a crab or a scorpion grabbing onto something. Figure 1 illustrates an example of a pincer complex bound to an iridium center atom. Pincer complexes have been found to be able to reduce unsaturated carbon based molecules such as CO_2, nitriles, amides, esters, olefins and alkynes [14]. They have been used in combination with a variety of different metals such as iridium [15], manganese

[16] and ruthenium [17]. The problem with these metal catalysts is that they use costly and precious metals [18], but research has been focusing on finding low-cost and non-precious alternatives. Recently, zinc has emerged as a promising candidate for this matter.

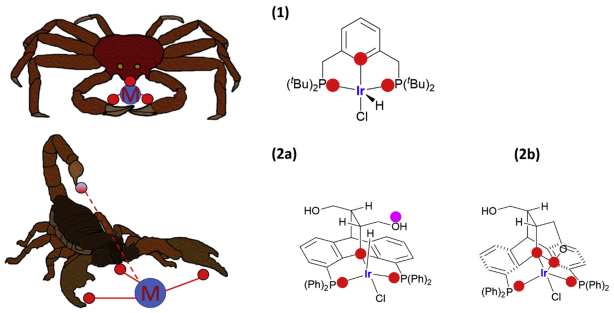

Figure 1: Comparison of a pincer-iridium complex to a crab and a scorpion to illustrate how pincer ligands bind to a metal center. Red dot illustrates the binding site. [15]

This research is focused on the non-transition metal zinc, which is believed to be a good option as a catalyst to further explore sustainable catalytic hydrogen storage technologies. The reason for this being its low toxicity and earth abundance. Research already suggests that zinc could work for semi-hydrogenation of alkynes [19]. The Global Warming Potential of zinc is about 113 times lower than that of ruthenium [20], which is a metal that is currently being used in both academic and industrial settings for hydrogenation reactions [21][22]. The electronic distribution of zinc's electron shells can be written as 2, 8, 18 and 2 (see Figure 2). In the fourth shell it has 2 valence electrons, which are the 4s electrons, and in the third shell 18 electrons, of which 10 are the electrons in the d-orbital [23]. The electronic configuration of zinc using the noble gas argon shorthand notation is

$$[\mathrm{Ar}]\ 3d^{10}\,4s^2$$

see Figure 2 for the complete configuration. Zinc has the ability to lose its 4s valence electrons because these are higher in energy [24]. It then becomes a cation with a 2+ charge with a filled d^{10} orbital.

Zinc complexes are flexible in coordination number, adapting tetrahedral, trigonal bipyramidal, square pyramidal and octahedral geometry[24]. It can range from 2-8 coordination depending on its ligands [26] and it is a medium-soft cation based on the hard-soft acid-base principle. This is reflected in the ligands that it binds with: hard donor atoms like nitrogen and oxygen and soft donor atoms like sulfur and phosphor. Zn^{2+} behaves like a lewis acid by accepting lone pairs from donor atoms into its empty 4s and 4p orbitals, this forms σ (sigma) bonds. When zinc is coordinated by hard or soft donors, it is prone to ligand exchange [27]. Given zinc's favorable coordination chemistry, recent studies have begun to explore its performance in hydrogenation reactions using PNP analogs [28]. PNP analogs are pincer ligands that bind to the center atom by two phosphorus and one nitrogen atom.

Reseach done on the zinc PNP pincer complexes has shown that these type of complexes can act as active catalyst. However, no information could be found on zinc complexes where all three donor

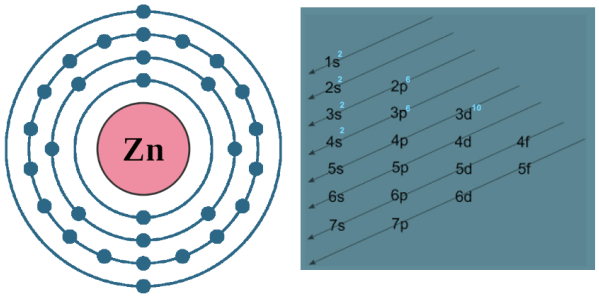

Figure 2: The left side of the figure illustrates the distribution of zinc's electrons across its atomic orbitals [23]. The corresponding electron configuration is shown on the right [25] and is written as:

$$1s^2\ 2s^2\ 2p^6\ 3s^2\ 3p^6\ 4s^2\ 3d^{10}$$

atoms bind simultaneously. For example, PNP-zinc complexes have shown their ability to activate N-H and H-H bonds via (de)aromatization with the help of hemilability of one phosphorus atom (see Figure 3) [29]. Hemilability is the ability of a ligand arm to reversibly detach from the metal atom and therefore provide an open coordination site during a reaction [30]. This phenomenon is believed to enhance catalytic activity of metal complexes [30]. As a result, the system was capable of catalyzing the hydrogenation of imines and ketones following bond activation and hemilability (Figure 3).

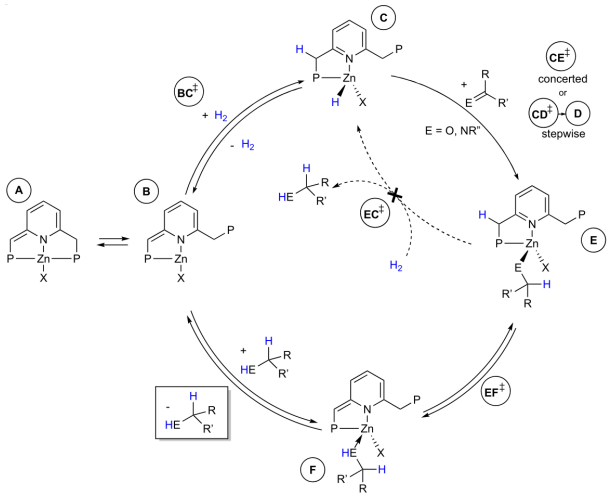

Figure 3: Zinc pincer complex showing hemilability of one of the phosphorus arms (A and B) allowing bond activation of H-H (B to C) and hydrogenation of imines and ketones (C to E) [29].

Recent research further demonstrates that hydrogenation reactions with three-coordinate zinc complexes as catalysts, supported by bidentate PNP and PN ligands with an R group like hydrogen

or methyl, are enhanced compared to their PNP analogs (Figure 4) [28].

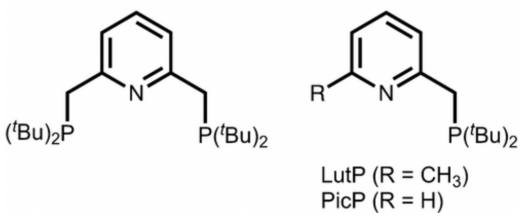

Figure 4: On the right side an example of a PNP analog. On the left side a PN ligand with R group

The synthesis of these zinc complexes are quite challenging, often facing problems during the isolation of the pure compounds [28]. Expensive chemicals, large amounts of resources and advanced skills are required to successfully synthesize these type of complexes. Therefore, it is convenient to use computational methods as a fast and effective way to screen the complexes for activity, stability and thermodynamic properties before synthesizing them. Computational catalysis is actively used for this purpose, but there are some challenges attached to this method. "The issue of accuracy" is one of these. There is a challenge regarding the accuracy of the methodology to determine the electronic structure of a system and the quality of the chemical model [31]. It is not easy to simultaneously reach these accuracies. That said, there are some methodological applications that simplify/approximate the model chemical systems and their electronic structures. One largely use example of this application is that of Density Functional Theory (DFT). It numerically approaches the Schrödinger equation to find the electronic structure of molecules [32]. This method uses exchange-correlation functionals and basis sets to find a balance between accuracy and computational cost.

1.2 Research Objective and Scope

This project is an *in silico* screening of zinc pincer complexes for hydrogen storage via homogeneous hydrogenation of pyridine. For a catalytic reaction to take place, the substrate must first bind to the catalyst complex. Thus, the main question to be answered is the following: Are zinc pincer complexes thermodynamically capable of binding pyridine as a substrate and stabilizing the resulting complex? This will be answered by investigating the preferred coordination geometries of Zn(II) in complexes with pincer ligands having PNP and NNN backbones, as well as examining if these complexes show hemilability and if so, how does this influence the thermodynamic stability of these Zn(II) complexes. Furthermore, the influence of different R groups on the ligand backbone will also be examined. Additionally, it will be investigated wether the pincer ligand binds strongly enough to not be substituted by pyridine. An octahedral zinc pincer complex was taken as an initial guess for the starting complex.

The scope of this project will be to identify optimal complexes that have favorable Gibbs free energy ($\Delta G_{\text{binding}}$) for the binding of pyridine to the zinc center by using DFT calculations.

The main hypothesis for this project is that zinc will bind to the pincer complexes with hemilability of one of the donor atoms. Moreover, it is expected that pyridine can bind favorably to the zinc complexes. Another hypothesis is supported by DFT optimization studies [33] which shows that zinc complexes with strong ligands or neutral donor atoms relax into tetrahedral shapes, even when starting with octahedral inputs. Furthermore, tetrahedral geometry is shown to have a low energy configuration when coordinated to one acidic or two or more neutral ligands [33]. Therefore it is believed that during DFT optimization of the octahedral complexes these structures will have dissociation of atoms and form tetrahedral complexes instead.

2 MODELS AND METHODS

The reaction energy for the binding of pyridine is calculated using Equation 1, which is based on the mass balance of the chemical reaction. These values are obtained from DFT calculations.

$$\Delta G_{\text{binding}} = G_{\text{complex with pyridine}} + G_{\text{dissociated ligand}} - G_{\text{complex}} - G_{\text{pyridine}} \tag{1}$$

First 3D structures of the pincer ligand complexes were created to calculate their Gibbs free energy. The geometry optimization was then performed to recalculate the energy of the complex and proceed with the reaction energy. The hemilability of these complexes was also analyzed during the optimization. Further explanation of the steps taken are discussed in the following paragraphs.

2.1 Ligand Design

Ligands (see Figure 5) were first drawn in ChemMarvin, a universal chemical editor, to later extract their SMILES code, which is a representation code for molecular structures [34]. Next, files with xyz Cartesian coordinates of the complexes were generated using the SMILES of the ligands. The files generated are directly suitable for quantum chemical computations. The Python scripts with the epic-mace package were used. MACE is an automated computational workflow that transforms SMILES code into 3D structures of all feasible stereoisomers for octahedral and square planar complexes [34]. MACE was used to generate the xyz files of the complexes [PNP-Zn-L] and [NNN-Zn-L] with all R groups, where L = two hydrogens (H=hydrogen) and pyridine (Pyr). R groups are uniformly substituted for each backbone. MACE was opened in Command Line Interface (CLI) by using the code 'epic-mace-quickstart' and directly after 'nano mace_input.yaml'. Avogadro and Chemcraft were used as vizualization programs for the files generated. After generating the xyz files, the pyridine molecule was manually substituted for carbonyl (CO) in Avogadro to later on do DFT calculations on all isomers for the complexes with pyridine and with CO. This is because different isomers can have different energies and the binding energie is calculated using the most thermodynamically stable isomer (major isomer) with the lowest energy value obtained.

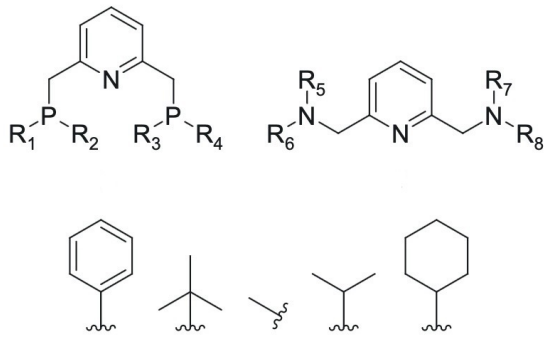

Figure 5: Molecular structures of the PNP (upper left) and NNN (upper right) pincer ligand backbones. R groups are the following: phenyl (phe), tert-butyl (t-but), methyl (me), isopropyl (iso), and cyclohexane (cy).

2.2 Density Function Theory Calculations

Geometry optimization and frequency calculations of the PNP and NNN complexes were performed with DFT to calculate the energy minima of the complexes. This was done using ORCA quantum chemistry software [35] and the national supercomputer *Snellius* [36]. Input files for ORCA were manually created by using ORCA keywords and the coordinates from the xyz files. See Table 1 for a summary of the keywords that were used. This combination of keywords have been observed to work successfully for metal-complexes and have a low computational cost [37]. All thermochemistry calculations were carried out with standard conditions of 298.15 Kelvin and 1.00 atmospheric pressure. Additionally, calculations were performed in vacuo (complexes in gas phase) using 24 processor cores with 2000 Mega bytes per core. The limited time set for a job was 24 hours, but the jobs were completed within two to five hours. After running the input files in ORCA, various files were generated, including files with densities, errors committed during running, new Cartesian coordinates, thermodynamic calculations etc.

Purpose	**Keyword**	**Explanation**
Optimization	`OPT`	Stands for Optimize geometry. Used to find the most stable structure of a molecule.
Frequency Calculation	`FREQ`	Performs frequency calculations to verify that the optimized structure is a true minimum and to compute thermodynamic properties such as entropy and Gibbs free energy.
Functional	`PBE0`	A hybrid functional combining Generalized Gradient Approximation (GGA) and exact exchange, it is believed to strike a balance between accuracy and computational cost for metal-ligand complexes
Dispersion Correction	`D3BJ`	Used for dispersion correction in DFT calculations. It improves accuracy for noncovalent interactions.
Basis Set	`def2-SVP`	Used for the approximation of the wavefunctions of electrons while offering a balance between accuracy and computational efficiency

Table 1: Purpose, keywords and explanation of ORCA input settings used in the computational workflow [38] [39].

Note that for zinc complexes other keywords for functionals of the type hybrid-Generalized Gradient Approximation (GGA) can be used instead of PBE0, which is what is currently being used in the research group. For example B3LYP have been found to have a good performance for the topology of the system, but it comes with drawbacks in fields like electron affinities [40].

2.3 Data Analysis

The first step of data analysis was checking the file with the errors commited during the calculations to make sure the calculations were done correctly. These files are called 'slurm-*batchnumber.out*'. If the calculations were successful the next step was to check the geometry of the complex, this was crucial due to the hypothesis that the octahedral geometry could change to another geometry. This step was done by opening the new cartesian files in ChemCraft and visualizing the structure

to check for geometry and hemilability. When geometry changed or hemilability was present, three new files were generated to reoptimize the structure for PNP backbone. The first one was an input file for ORCA with the new xyz coordinates to run this again, the reason for this was to find an even lower minima in energy if this existed. Second and third files were input files where the structures showed N and P hemilability, this was to check if hemilability was indeed present after reoptimization and to see the difference between the energy of these two. For NNN only one file for reoptimization was sent due to the first optimization giving only one type of geometry. Later on it was seen in ChemCraft that some of these structures (starting complexes) show hemilability, but reoptimization for hemilability was not done due to time limitation.

A visualization of the approach taken can be seen in Figure 6.

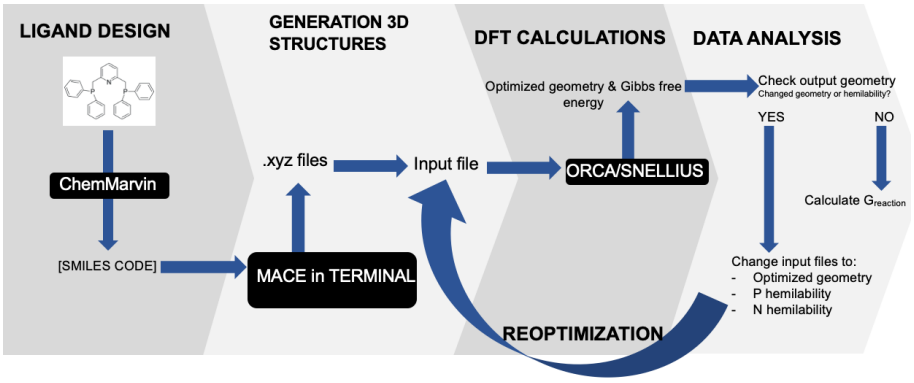

Figure 6: A path of the approach followed.

3 RESULTS & DISCUSSION

This section provides a detailed analysis of the results for the PNP and NNN backbones, including the thermodynamics of pincer ligand dissociation and the binding of two pyridine molecules.

3.1 Geometry optimization

MACE generated two configurations for all R groups in both PNP and NNN backbones, except for phenyl. This R group gave only one configuration. See Figure 7 for an illustration of the configurations. The difference in these configurations is the position of the hydrides attached to the zinc metal center. They are positioned in the cis or trans configuration. The ligand adjusts itself depending on whether the complex adopts a cis or trans configuration, resulting in different spatial arrangements. The configuration found for R=phenyl was cis. Later on it was noticed that MACE gives more configurations for R=phenyl when running CO complex, which are [PNP-Zn-L] where L = H, H, CO.

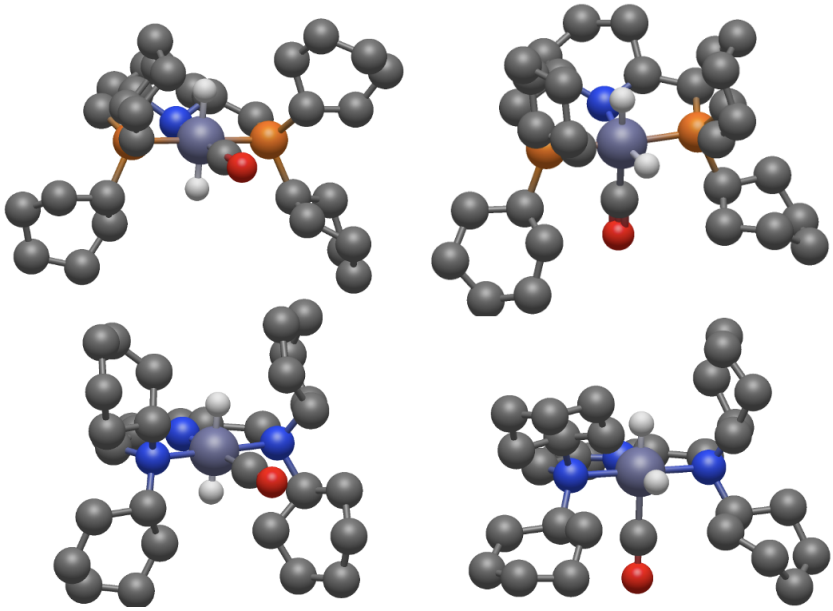

Figure 7: Two configurations created by MACE for PNP-cy and NNN-cy. First row of figures are PNP structures and second row are NNN structures. Left side is trans configuration and right side is cis configuration regarding the position of the hydride ligands. Hydrogen atoms bound to the ligand are not shown. Color code for atoms: grey=carbon, orange=phosphorus, purple= zinc, blue=nitrogen, white=hydrogen and red=oxygen

Geometry optimization using DFT of the PNP and NNN zinc complexes showed that CO ligand dissociates from the zinc metal center. CO donates electrons to zinc via σ donation. This ligand uses π-backbonding to stabilize metal-CO bond. However, due to zinc's filled d^{10} orbital, it cannot easily donate its electrons into CO's pi antibonding orbital. This explains the dissociation of CO from zinc. For this reason, no further DFT calculations (reoptimization) were ran using CO as a

ligand. Additionally, all PNP starting complexes started with an octahedral structure but relaxed into tetrahedral geometries, except for one PNP-cy isomer which had a 3 coordinated structure. The products of PNP-R show 5 coordinated geometries when using phenyl and tert-butyl as R group. All other PNP-R product complexes have tetrahedral geometries. For NNN-R, the starting complexes are 3, 4 and 5 coordinated. NNN-phe was the only complex that showed successful binding of pyridine. All other NNN-R products show different geometries, but none of them show pyridine binding (Figure 8). These results suggest that pyridine binding is more favorable when using a PNP backbone rather than an NNN backbone for zinc complexes.

This is believed to be due to phosphorus atoms being less electronegative than nitrogen atoms, making phosporous atoms better σ donors and therefore easier to stabilize the complex when additional ligands are added to it. In contrast, nitrogen atoms are more electronegative and they create a crowded and high electron density environment around zinc, thus making the binding of pyridine more difficult.

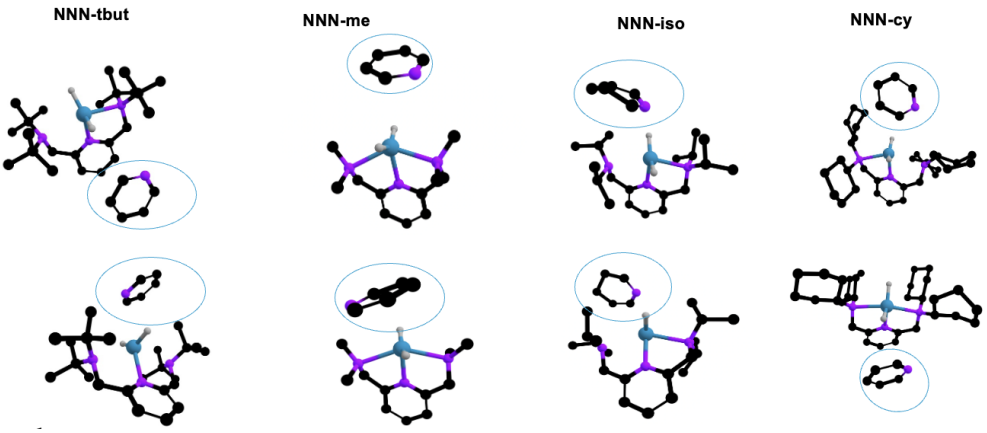

Figure 8: Optimized structures of NNN-R products per MACE configuration where pyridine binding was not favorable. Pyridine is encircled in blue. Hydrogen atoms bound to ligands are not showed. Color code for atoms: black=carbon, blue= zinc, purple= nitrogen and grey=hydrogen

Figure 8 shows the starting complexes, where pyridine is weakly bound to them via Van der Waals interactions. NNN-tbut and NNN-cy show hemilability of one of the N arms in the starting complex. Unfortunately, due to timelimit the energie values for the different hemilabile structures could not be calculated.

3.2 Analysis of PNP-R

This section focuses on the analysis of the structures with a PNP backbone. MACE gave 2 configurations per R group for the PNP backbone , except for phenyl which only had one. These configurations were then investigated using ORCA, which resulted in the identification of two isomers in the starting complex per R group and dissociation of the CO ligand. The isomers exhibit either N- or P-hemilability (see Figure 9). In one isomer (PNP-cy), only P-hemilability was observed with a complete dissociation of the N atom. In this complex, the ligand behaves more like a bidentate ligand with hemilability of one phosphorus arm.

In these PNP-complexes both the phosphorus and nitrogen atom can dissociate in the starting complexes to establish a three or four coordinated state. Thus, complexes with PNP backbones demonstrated a flexible ligand environment.

Figure 9 illustrates that PNP-me and PNP-cy show higher energy differences between the starting complex isomers. For PNP-me the energy gap is 16 kJ/mol between the isomers, suggesting that both isomers may coexist in equilibrium but there is a stronger preference for PNP-me with P-hemilability. For PNP-cy with the N atom dissociated the energy difference between isomers is 51 kJ/mol. This energy gap is big enough to only find the lowest energy isomer in equilibrium. To futher support this statement, the Boltzmann ratio was calculated for this complex using equation 2. Boltzmann ratio gives the relative population ratio of a particular arrangement based on its energy difference [41]. This ratio was then normalized to percentages for an estimation of the probability for the population of one isomer at equilibrium. The percentage for the lowest energy isomer for PNP-cy was 100 %. Thus, only tetrahedral with N atom dissociated is expected to be present at equilibrium for PNP-cy. These results further suggest that zinc pincer complexes with PNP backbone do not prefer three coordinated structures.

In contrast, the energy difference between the reactant isomers is small for PNP-phe, PNP-tbut, and PNP-iso, indicating that no single isomer is strongly favored allowing dynamic interconversion between these.

$$\frac{N_2}{N_1} = e^{-\frac{\Delta G}{RT}} \tag{2}$$

Boltzmann ratio: N_2 stands for the higher energy isomer and N_1 for the lower energy isomer. R stands for the gas constant, $8.314\,\mathrm{J\,mol^{-1}\,K^{-1}}$. The temperature is 298.15 Kelvin, which is based on the temperature of the DFT calculations.

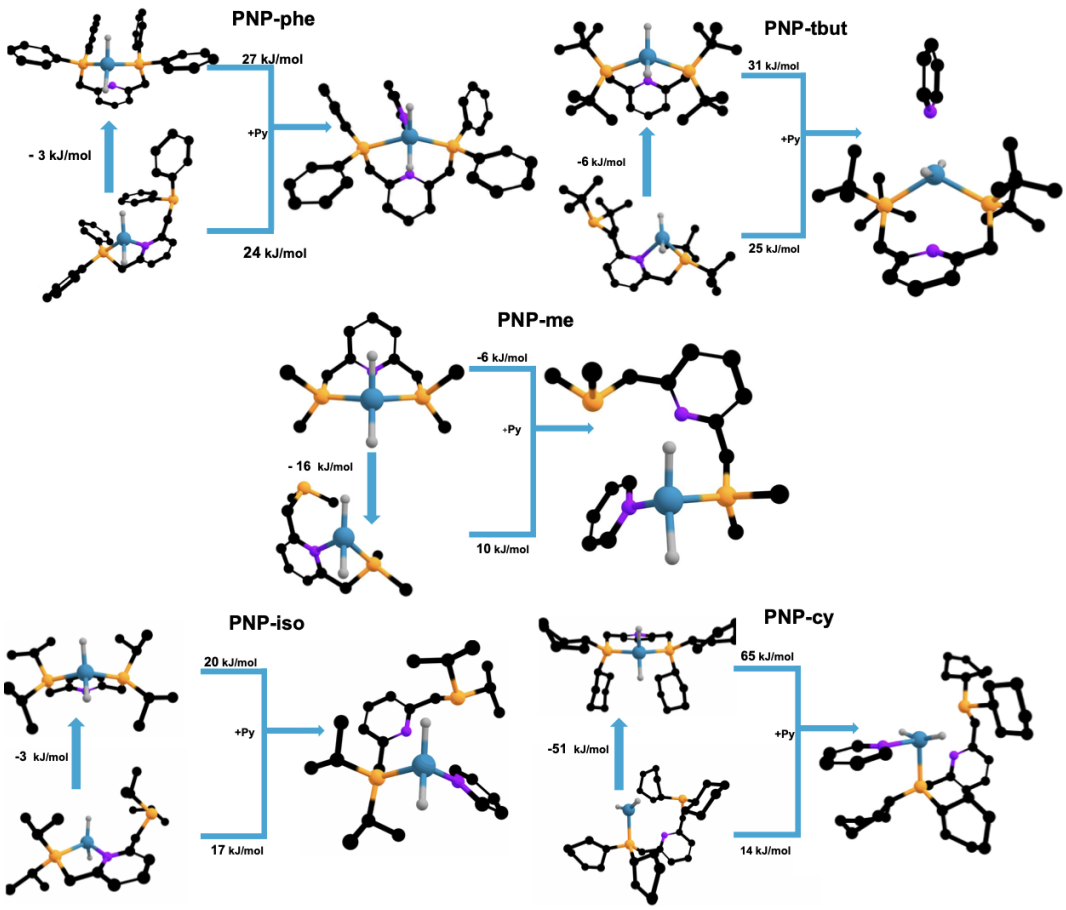

Figure 9: Pyridine binding reaction per R group with isomers for starting complex. Blue arrow between starting complexes points to the most stable isomer. Hydrogen atoms bound to ligands are not showed. Color code for atoms: black=carbon, blue= zinc, orange= phosphorus and grey=hydrogen

The results from Figure 9 show that the tetrahedral PNP starting complexes with the nitrogen atom dissociated are the major isomers for all ligands except for PNP-me. This is believed to be because phosphorus atoms are strong sigma donors and zinc relies strongly on sigma donation due to its filled d10 orbital. Phosporous atoms are bigger than nitrogen atoms and they have a larger radius for their electron shell. Therefore, they can share electrons by sigma donation easier than nitrogen atoms. Thus, it is logical that PNP complexes with both phosphorus atoms bound are favored.

Pyridine binds to PNP zinc complexes through different coordination modes. The reaction with pyridine starts from a starting complex with N-hemilability and it can directly bind pyridine (like PNP-phe or PNP-tbut) or it can form a P hemilabile structure and create a binding site for

pyridine (PNP-me, PNP-iso and PNP-cy). This last result is similar to the results shown in the activation of H-H bonds with tetrahedral PNP-zinc complexes were the P atom shows hemilability and therefore creates a binding site for one H atom [29]. This example was mentioned in Figure 3. Only in the case of PNP-me does the major isomer show P-hemilability. This distinct behavior is due to the methyl group being the smallest R group, resulting in less steric hindrance and lowest binding energy. As a consequence, both the P and N donor atoms are able to coordinate to the zinc center simultaneously in the major isomer. This difference did not influence the hemilability in the product of PNP-me when comparred to PNP-iso and PNP-cy products.

It is important to point out that the product of PNP-tbut has no bond between the pyridine and the zinc metal center. According to Figure 10, this complex exhibits a pyridine-metal bond length of 2.72 Å, which falls outside the range observed for the other products (2.16–2.42 Å). Despite this, it is still believed that pyridine is weakly bound to PNP-tbut because the nitrogen atom of the pyridine is positioned directly above the zinc center. It is possible that this bond exists, but its length falls outside the range in which ChemCraft displays bonds.

Moreover, the highest binding energy, that of PNP-cy with a value of 65 kJ/mol, has a binding energy of 2.28 Å. The lowest binding energy value corresponds to PNP-me, with a value of 10 kJ/mol and a bond length of 2.16 Å. Interestingly this is the same bond length for PNP-iso, but the binding energy of this complex is twice that of PNP-me. These findings indicate that the binding length alone does not fully explain the favorability of pyridine coordination to PNP zinc complexes.

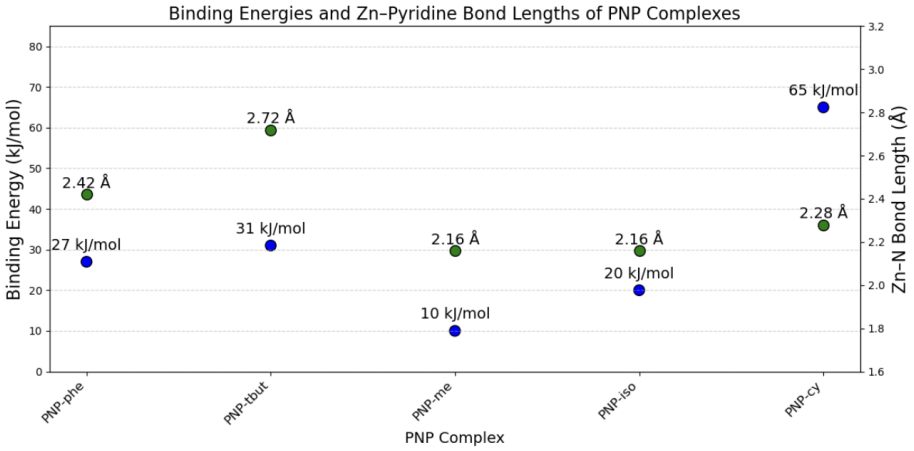

Figure 10: $\Delta G_{\text{binding}}$ of PNP-R complexes and their corresponding binding length of zinc–pyridine. The binding energies are calculated using the most stable starting complex isomer as reference.

Furthermore, both PNP-phe and PNP-tbut have a five coordinated trigonal bipyramidal structure for the complex with pyridine, however the bond length of PNP-phe is shorter than that of PNP-tbut. This is believed to be due to phenyl groups being planar and being able to rotate around their P-C bonds, which allows them to accomodate when ligands are bound close to them. In contrast, tert-butyl groups are bulky and cone-shaped, causing more steric hindrance around the metal center. When comparing these two groups in the same position in the backbone analysed,

tert-butyl groups limit the access for new ligands to bind to the metal center more than phenyl groups do. This explains the high zinc-pyridine bond length of PNP-tbut.

Additionally, PNP-phe starting complex with N hemilability has a bite angle of 98 degrees, which is smaller than all other starting complexes with N hemilability (see Figure 11). This is believed to be due to PNP-phe exhibiting π–π interactions between the two phenyl groups facing each other. The strong π–π interactions between the phenyl rings draw them closer together, resulting in a small bite angle between the phosphorus atoms to which they are attached. This phenomenon of π–π interactions was also observed for the PNP-phe complex with pyridine bound.

Pyridine bound to the complex in between two phenyl rings creating π–π stacking interactions. A clear trend is observed for the bite angle of the isomers of the starting complexes that have N atom dissociated (bite angle is calculated from P-P). The bite angle is around 120 degrees, with the exception of PNP-phe. Furthermore, the isomers with P atom dissociated also have a trend for a bite angle between P and N atom of around 78 degrees.

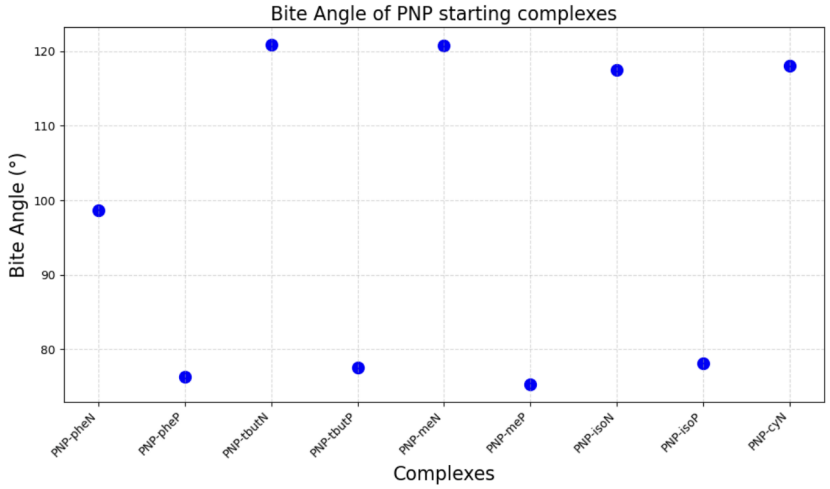

Figure 11: Bite angles of PNP-R starting complex isomers, where 'N' in the name refers to the isomer with the N atom dissociated and the angle measured between P-zinc-P. Letter P in the name refers to P atom dissociated and a bite angle between P-zinc-N.

3.3 Analysis of NNN-R

For NNN-R different geometries can be observed for starting complexes. NNN-Phe and NNN-tbut have three coordinated structures, whereas NNN-me, NNN-iso and NNN-cy have five coordinated structures (see Figure 12).

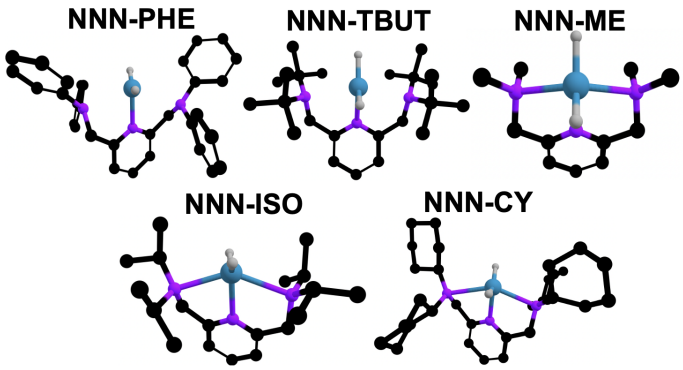

Figure 12: Optimized structures of NNN-R starting complexes. Hydrogen atoms bound to ligand are not showed. Color code for atoms: black=carbon, blue= zinc, purple= nitrogens and grey=hydrogen

As mentioned in section 3.1, only NNN-phe showed a structure in which pyridine was bound. Geometry optimization gave only one isomer for the reactant of this complex, which turned out to be a 3 coordinated structure where zinc was bound to the middle nitrogen atom of the NNN backbone. During the reaction with pyridine, one of the hydrides that was bound to the zinc center migrated to one of the phenyl rings in the backbone (Figure 13). The product is a 4 coordinated structure of zinc bound to 3 nitrogen atoms and one hydride with a binding energy reaction of 76 kJ/mol. The hydrogen migration indicates that the hydride in the starting complex is highly reactive, causing it to hydrogenate the aromatic benzene ring.

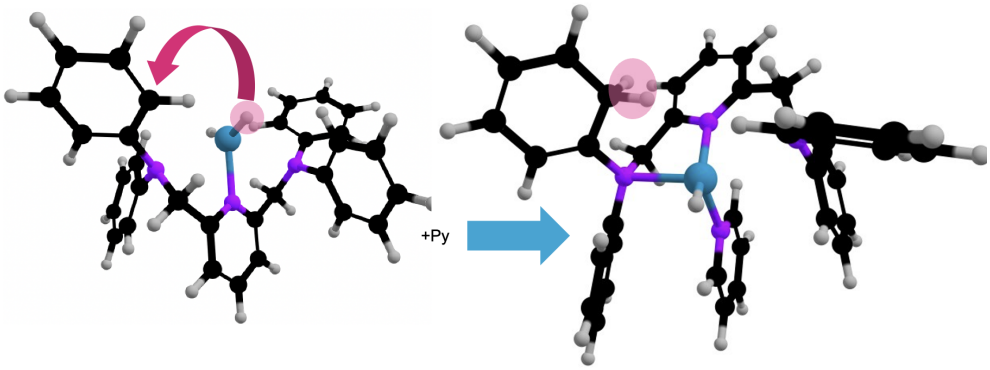

Figure 13: Reaction of NNN-phe with pyridine. Pink arrow shows the hydride migration.

Aromaticity was disrupted in the phenyl ring, causing a shift in electron density. This statement

was further supported by a relatively negative charge of -0.135 e (elementary charge) on the carbon atom with only three bonds in the phenyl ring (showed in pink circle in Figure 13). This implies that a mechanism in Figure 14 likely occured. Pyridine bound to the side where the phenyl groups still had aromaticity, probably to maintain π–π stacking interactions like seen before in PNP-phe product.

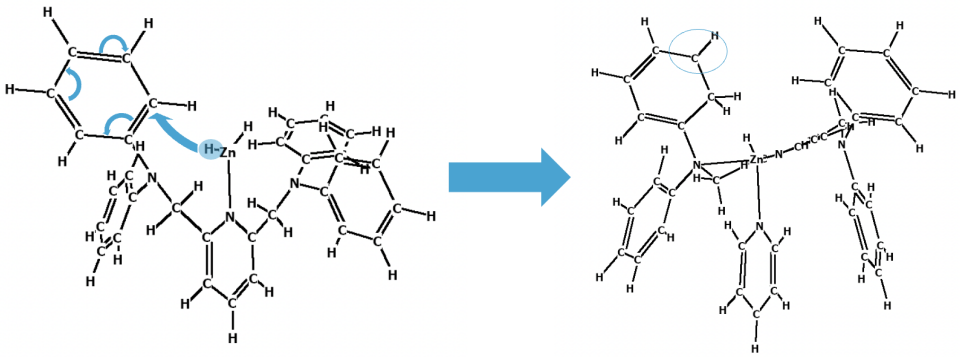

Figure 14: Left: Mechanism for the migration of the hydride ligand. Right: Carbon atom with a negative charge encircled in blue.

It is believed that the reason only one complex showed the binding of pyridine to NNN complex is due to the three electron rich nitrogen atoms in the backbone. Nitrogen is considered harder than zinc, making the binding of multiple nitrogen atoms to zinc difficult. This phenomenon was also observed in PNP backbone, where N dissociation was mostly preffered in both reactants and products. Additionally, when zinc is already bound to numerous nitrogen atoms it gets a high electron density around it. Furthermore, nitrogen atoms are electronegative, meaning that they hold their electrons tighther therefore creating a crowded chemical environment around the zinc metal center.

These facts suggest that for NNN-phe, the key for pyridine binding was the hydride migration in the three coordinated structure. This phenomenon lowered the electron density around the zinc atom, allowing pyridine to bind with its electron pair. The positive reaction energy illustrates that this reaction is not thermodynamically favored.

3.4 Complete dissociation of pincer ligand

In this section, the thermodynamics of the interchange of the pincer ligand and pyridine are addressed. The reaction studied was that of two pyridine molecules substituting the original pincer ligand in the most stable starting complex, see the following reaction. The letter 'L' represents the pincer ligand and 'Pyr' represents pyridine.

$$L\mathrm{ZnH_2} + 2\,\mathrm{Pyr} \rightarrow L + \mathrm{Pyr_2ZnH_2} \tag{3}$$

Only in two NNN complexes was the binding of pyridine thermodynamically favored, these were NNN-phe and NNN-tbut (see Figure 15). This is logical, seeing that these complexes are 3

coordinated and zinc is bound to the pincer ligand only by one nitrogen atom. Additionally, all other NNN complexes were bound to the pincer ligand by all three nitrogen donor atoms, therefore making it difficult to dissociate all three donor atoms and bind pyridine.

It is important to take into account that the NNN complexes were not fully investigated for hemilability, therefore it is not known if NNN-me, NNN-iso and NNN-cy have lower energy isomers with hemilability which, supported by the results in this section, could have different values for the binding energy of this reaction.

Moreover, all PNP pincer complexes bind strong enough to resist substitution. This strong interaction is believed to be due to sigma donation of the phosphorus atoms.

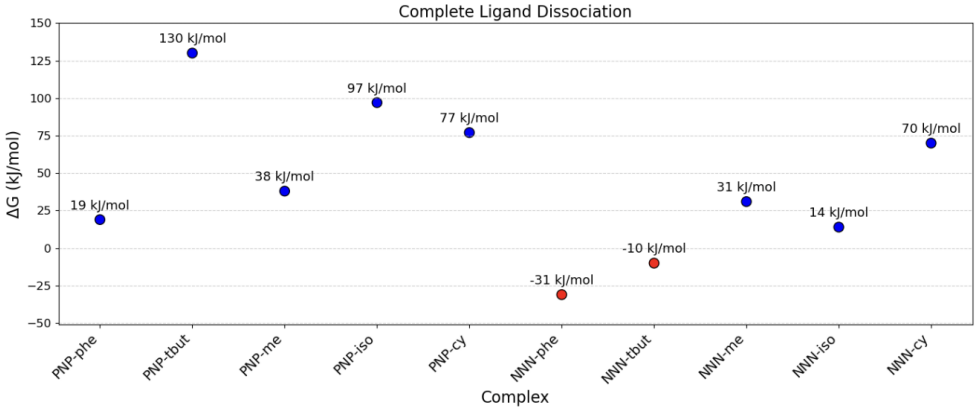

Figure 15: $\Delta G_{\text{binding}}$ of two pyridine molecules causing complete substitution of the pincer ligand.

These results suggest that even though PNP complexes can show hemilability of the P and the N arm, the full displacement of this ligand by two pyridine molecules is still unfavorable. In contrast, NNN complexes with 3 coordinated structures are thermodynamically suitable for the ligand substitution by two pyridine molecules.

4 CONCLUSION & RECOMMENDATIONS

This study explored zinc complexes with PNP and NNN pincer ligands using phenyl, tert-butyl, methyl, isopropyl, and cyclohexane as R groups. The goal was to analyse the thermodynamic feasibility of these complexes for the hydrogenation reaction of pyridine by calculating the binding energy of pyridine. It was found that zinc pincer complexes are not thermodynamically capable of binding pyridine as a substrate and stabilizing the resulting complex. Geometry optimization concluded that the CO ligand in the octahedral initial guess dissociated from the zinc center, indicating that CO is not a good ligand for PNP/NNN zinc pincer complexes. Additionally, PNP-R complexes showed a preference for tetrahedral geometry in both reactants and products. Nevertheless, exceptions like PNP-cy, PNP-tbut, and PNP-phe showed three and five coordinate environments. Both PNP-phe and PNP-tbut showed a trigonal bipyramidal structure. PNP-phe had the smallest bite angle within the N hemilabile PNP starting complexes, which is believed to be for π–π stacking interactions. Furthermore, NNN-R starting complexes showed both 3 and 5 coordinate geometries. These results showed how zinc pincer complexes are flexible in geometry coordination.

Additionally, it was found that PNP complexes have a flexible ligand environment and dynamic hemilability. Isomers with both P and N hemilability for PNP starting complexes can be both found in equilibrium due to their low energy difference between eachother, except for the 3 coordinated isomer of PNP-cy, this was confirmed using the Boltzmann ratio. This result suggests that three coordinated PNP zinc complexes are not stable. In contrast to all other PNP ligands, PNP-cy behaved more like a bidentate ligand, with hemilability of one P arm. Moreover, PNP with the smallest R group and lowest binding energy, methyl, was the only reactant with a major isomer showing P-hemilability, allowing both N and P atoms to bind simultaneously. Together, these observations highlight how the size of the R group can influence the stability and coordination mode of zinc complexes.

DFT results showed that pyridine binding is more favorable for PNP backbones than for NNN backbones, which is believed to be due to the better σ bonding of the phosphorus atom. All PNP complexes showed pyridine bound. In contrast DFT calculations for the NNN products showed that only NNN-phe formed a complex with pyridine bound. This is believed to be the result of a hydride migration to one of the phenyl rings, which hydrogenates the aromatic benzene ring, lowering the electron density around zinc, making the chemical environment less crowded and enabling pyridine coordination. Outcome of calculations showed that all reactions with pyridine are not thermodynamically feasible. The final part of this study involved the full substitution of the pincer ligand by two pyridine molecules which revealed that all complexes bind strong enough to resist substitution, with the exception of three coordinated NNN-complexes. Interestingly, PNP complexes are both dynamic hemilabile and strongly bound to resist complete substitution by two subtrate molecules. This balance of flexibility and stability may be advantageous in catalytic systems.

Future work could focus on exploring whether having a major isomer with N-hemilability that rearranges into a P-hemilabile form could create a favorable path for pyridine binding. Although such rearrangements in this study led to positive reaction energies, they might still provide mechanistic insight into dynamic hemilability and binding cooperativity.

Additionally, more LOHCs could be research for the binding and stabilization of PNP and NNN zinc complexes. For PNP pincer ligand, it would be insightful to investigate more types of N-heterocycles, with a focus on P,N-heterocycles.

This is due to the observation of PNP-zinc complexes showing preference when binding to P atoms rather than N atoms. P,N-heterocycles could be explored to see whether they can maintain a low reaction enthalpy (like N-heterocycles) while also allowing the phosphorus atom to bind and unbind reversibly. This might be promising because phosphorus is known to exhibit hemilability with zinc complexes, and this behavior could potentially be translated into a dynamic coordination mode of the P,N-heterocycles in combination with the hemilability of the phosphorus arm in a PNP zinc complex. If such reversible P–Zn binding is possible, it could allow a P,N-heterocycle to bind as a substrate following hemilability of one phosphorus atom in the PNP backbone, potentially leading to a more thermodynamically favorable binding environment and energy.

Furthermore, due to NNN-phe portraying hydrogenation in one of the phenyl rings, it is reasonable to explore in more detail the mobility and reactivity in this complex. This could give more information about the chemistry of aromatic hydrocarbons as R groups for NNN ligands in zinc complexes.

Lastly, because all calculations were performed in the gas phase, it is recommended to repeat the screening of this project in a solvent model, perhaps pyridine, to understand solvent effects on pyridine binding and ligand substitution. This change will give a more realistic insight into how these complexes behave under actual catalytic conditions.

References

[1] M. Roser and H. Ritchie, "How has world population growth changed over time?" en, *Our World in Data*, Jun. 2023. [Online]. Available: https://ourworldindata.org/population-growth-over-time (visited on 06/10/2025).

[2] *Fritz Haber – Facts - NobelPrize.org*. [Online]. Available: https://www.nobelprize.org/prizes/chemistry/1918/haber/facts/ (visited on 06/10/2025).

[3] R. Steinberger-Wilckens and B. Sampson, "Chapter 8 - Market, Commercialization, and Deployment—Toward Appreciating Total Owner Cost of Hydrogen Energy Technologies," in *Science and Engineering of Hydrogen-Based Energy Technologies*, P. E. V. de Miranda, Ed., Academic Press, Jan. 2019, pp. 383–403, ISBN: 9780128142516. DOI: 10.1016/B978-0-12-814251-6.00008-3. [Online]. Available: https://www.sciencedirect.com/science/article/pii/B9780128142516000083 (visited on 06/10/2025).

[4] MERYT, *The Catalyst That Changed the World: The Story of Haber-Bosch Ammonia Catalyst*, en, Aug. 2024. [Online]. Available: https://meryt-chemical.com/the-catalyst-that-changed-the-world-the-story-of-haber-bosch-ammonia-catalyst/ (visited on 06/10/2025).

[5] *14.7: Catalysis*, en, Feb. 2015. [Online]. Available: https://chem.libretexts.org/Bookshelves/General_Chemistry/Map%3A_Chemistry_-_The_Central_Science_(Brown_et_al.)/14%3A_Chemical_Kinetics/14.07%3A_Catalysis (visited on 06/10/2025).

[6] LumenLearning, "Catalysis," en, [Online]. Available: https://uen.pressbooks.pub/introductorychemistry/chapter/catalysis/ (visited on 06/30/2025).

[7] *Catalysts: At the core of efficient industrial processes*. [Online]. Available: https://www.topsoe.com/blog/catalysts-at-the-core-of-efficient-industrial-processes (visited on 06/10/2025).

[8] U. S. Meda, N. Bhat, A. Pandey, K. N. Subramanya, and M. A. Lourdu Antony Raj, "Challenges associated with hydrogen storage systems due to the hydrogen embrittlement of high strength steels," *International Journal of Hydrogen Energy*, vol. 48, no. 47, pp. 17 894–17 913, Jun. 2023, ISSN: 0360-3199. DOI: 10.1016/j.ijhydene.2023.01.292. [Online]. Available: https://www.sciencedirect.com/science/article/pii/S036031992300530X (visited on 06/10/2025).

[9] *Hydrogen Storage — Department of Energy*. [Online]. Available: https://www.energy.gov/eere/fuelcells/hydrogen-storage (visited on 06/27/2025).

[10] M. Besora and F. Maseras, "Chapter Six - Computational insights into metal-catalyzed asymmetric hydrogenation," in *Advances in Catalysis*, ser. Metal-catalyzed Asymmetric Hydrogenation: Evolution and Prospect, M. Diéguez and A. Pizzano, Eds., vol. 68, Academic Press, Jan. 2021, pp. 385–426. DOI: 10.1016/bs.acat.2021.08.006. [Online]. Available: https://www.sciencedirect.com/science/article/pii/S0360056421000067 (visited on 06/10/2025).

[11] A. Lin and G. Bagnato, "Revolutionising energy storage: The Latest Breakthrough in liquid organic hydrogen carriers," *International Journal of Hydrogen Energy*, vol. 63, pp. 315–329, Apr. 2024, ISSN: 0360-3199. DOI: 10.1016/j.ijhydene.2024.03.146. [Online]. Available: https://www.sciencedirect.com/science/article/pii/S0360319924009789 (visited on 06/27/2025).

[12] *Heterocyclic compound — Definition, Examples, Structure, Nomenclature, Types, & Facts — Britannica*. [Online]. Available: https://www.britannica.com/science/heterocyclic-compound (visited on 06/27/2025).

[13] S. A. Stepanenko, D. M. Shivtsov, A. P. Koskin, *et al.*, "N-Heterocyclic Molecules as Potential Liquid Organic Hydrogen Carriers: Reaction Routes and Dehydrogenation Efficacy," en, *Catalysts*, vol. 12, no. 10, p. 1260, Oct. 2022, ISSN: 2073-4344. DOI: 10.3390/catal12101260. [Online]. Available: https://www.mdpi.com/2073-4344/12/10/1260 (visited on 06/27/2025).

[14] K. K. Manar, J. Cheng, Y. Yang, X. Yang, and P. Ren, "Promising Catalytic Application by Pincer Metal Complexes: Recent Advances in Hydrogenation of Carbon-Based Molecules," en, *ChemCatChem*, vol. 15, no. 15, e202300004, Aug. 2023, ISSN: 1867-3899. DOI: 10.1002/cctc.202300004. [Online]. Available: https://chemistry-europe-onlinelibrary-wiley-com.tudelft.idm.oclc.org/doi/10.1002/cctc.202300004 (visited on 04/29/2025).

[15] A. V. Polukeev and O. F. Wendt, "Iridium complexes with aliphatic, non-innocent pincer ligands," *Journal of Organometallic Chemistry*, Special Issue dedicated to Prof. Irina Beletskaya, vol. 867, pp. 33–50, Jul. 2018, ISSN: 0022-328X. DOI: 10.1016/j.jorganchem.2017.12.009. [Online]. Available: https://www.sciencedirect.com/science/article/pii/S0022328X17306940 (visited on 06/10/2025).

[16] W. Yang, "Activation, Reactivity and Dynamics of Manganese Pincer Complexes in Hydrogenation Catalysis," en, 2022. DOI: 10.4233/c40b1935-c5f1-4887-9185-d514ef408d6f. [Online]. Available: https://repository.tudelft.nl/record/uuid:c40b1935-c5f1-4887-9185-d514ef408d6f (visited on 05/12/2025).

[17] H. A. Younus, N. Ahmad, W. Su, and F. Verpoort, "Ruthenium pincer complexes: Ligand design and complex synthesis," *Coordination Chemistry Reviews*, vol. 276, pp. 112–152, Sep. 2014, ISSN: 0010-8545. DOI: 10.1016/j.ccr.2014.06.016. [Online]. Available: https://www.sciencedirect.com/science/article/pii/S0010854514001830 (visited on 06/27/2025).

[18] *Is Palladium a Precious Metal? — Palladium Bullion — APMEX*, en-US, Aug. 2023. [Online]. Available: https://learn.apmex.com/learning-guide/is-palladium-precious-metal/ (visited on 06/10/2025).

[19] G. J. Baker, A. J. P. White, I. J. Casely, D. Grainger, and M. R. Crimmin, "Catalytic, Z-Selective, Semi-Hydrogenation of Alkynes with a Zinc–Anilide Complex," *Journal of the American Chemical Society*, vol. 145, no. 13, pp. 7667–7674, Apr. 2023, ISSN: 0002-7863. DOI: 10.1021/jacs.3c02301. [Online]. Available: https://doi.org/10.1021/jacs.3c02301 (visited on 06/10/2025).

[20] P. Nuss and M. J. Eckelman, "Life Cycle Assessment of Metals: A Scientific Synthesis," en, *PLOS ONE*, vol. 9, no. 7, e101298, Jul. 2014, ISSN: 1932-6203. DOI: 10.1371/journal.pone.0101298. [Online]. Available: https://journals.plos.org/plosone/article?id=10.1371/journal.pone.0101298 (visited on 05/13/2025).

[21] P. Sánchez, M. Hernández-Juárez, N. Rendón, *et al.*, "Hydrogenation/dehydrogenation of N-heterocycles catalyzed by ruthenium complexes based on multimodal proton-responsive CNN(H) pincer ligands," en, *Dalton Transactions*, vol. 49, no. 28, pp. 9583–9587, Jul. 2020, ISSN: 1477-9234. DOI: 10.1039/D0DT02326D. [Online]. Available: https://pubs.rsc.org/en/content/articlelanding/2020/dt/d0dt02326d (visited on 06/10/2025).

[22] N. Tyagi, G. Borah, P. Patel, *et al.*, "Recent Advances in Ru Catalyzed Transfer Hydrogenation and Its Future Perspectives," en, in *Ruthenium - An Element Loved by Researchers*, IntechOpen, May 2021, ISBN: 9781839629174. DOI: 10.5772/intechopen.96464. [Online]. Available: https://www.intechopen.com/chapters/75522 (visited on 06/10/2025).

[23] PK, *Zinc Electronic Configuration and Distribution in Shells*, en, Mar. 2023. [Online]. Available: https://enthu.com/blog/chemistry/zinc-electronic-configuration (visited on 07/07/2025).

[24] J. Tang, H. .-. Yin, and J. .-. Zhang, "Chapter One - Luminescent Zinc Complexes as Bioprobes for Imaging Molecular Events in Live Cells," in *Inorganic and Organometallic Transition Metal Complexes with Biological Molecules and Living Cells*, K. K.-W. Lo, Ed., Academic Press, Jan. 2017, pp. 1–53, ISBN: 9780128038147. DOI: 10.1016/B978-0-12-803814-7.00001-0. [Online]. Available: https://www.sciencedirect.com/science/article/pii/B9780128038147000010 (visited on 04/29/2025).

[25] *Zinc Zn (Element 30) of Periodic Table - Elements FlashCards*. [Online]. Available: https://newtondesk.com/zinc-element/ (visited on 07/07/2025).

[26] P. D'Angelo and V. Migliorati, "Solvation Structure of Zn2+ and Cu2+ Ions in Acetonitrile: A Combined EXAFS and XANES Study," *The Journal of Physical Chemistry B*, vol. 119, no. 10, pp. 4061–4067, Mar. 2015, ISSN: 1520-6106. DOI: 10.1021/acs.jpcb.5b01634. [Online]. Available: https://doi.org/10.1021/acs.jpcb.5b01634 (visited on 04/29/2025).

[27] D. T. Richens, "Ligand Substitution Reactions at Inorganic Centers," *Chemical Reviews*, vol. 105, no. 6, pp. 1961–2002, Jun. 2005, ISSN: 0009-2665. DOI: 10.1021/cr030705u. [Online]. Available: https://doi.org/10.1021/cr030705u (visited on 04/29/2025).

[28] S. Paul, P. Morgante, S. N. MacMillan, J. Autschbach, and D. C. Lacy, "Hydrogenative Catalysis with Three-Coordinate Zinc Complexes Supported with PN Ligands is Enhanced Compared to PNP Analogs," en, *Chemistry – A European Journal*, vol. 28, no. 40, e202201042, 2022, ISSN: 1521-3765. DOI: 10.1002/chem.202201042. [Online]. Available: https://onlinelibrary.wiley.com/doi/abs/10.1002/chem.202201042 (visited on 04/29/2025).

[29] M. Rauch, S. Kar, A. Kumar, L. Avram, L. J. W. Shimon, and D. Milstein, "Metal–Ligand Cooperation Facilitates Bond Activation and Catalytic Hydrogenation with Zinc Pincer Complexes," *Journal of the American Chemical Society*, vol. 142, no. 34, pp. 14 513–14 521, Aug. 2020, ISSN: 0002-7863. DOI: 10.1021/jacs.0c05500. [Online]. Available: https://doi.org/10.1021/jacs.0c05500 (visited on 04/29/2025).

[30] P. Braunstein and F. Naud, "Hemilability of Hybrid Ligands and the Coordination Chemistry of Oxazoline-Based Systems," en, *Angewandte Chemie International Edition*, vol. 40, no. 4, pp. 680–699, Feb. 2001, ISSN: 14337851. DOI: 10.1002/1521-3773(20010216)40:4<680::AID-ANIE6800>3.0.CO;2-0. [Online]. Available: https://onlinelibrary.wiley.com/doi/10.1002/1521-3773(20010216)40:4%3C680::AID-ANIE6800%3E3.0.CO;2-0 (visited on 04/17/2025).

[31] K. D. Vogiatzis, M. V. Polynski, J. K. Kirkland, *et al.*, "Computational Approach to Molecular Catalysis by 3d Transition Metals: Challenges and Opportunities," en, *Chemical Reviews*, vol. 119, no. 4, pp. 2453–2523, Feb. 2019, ISSN: 0009-2665, 1520-6890. DOI: 10.1021/acs.chemrev.8b00361. [Online]. Available: https://pubs.acs.org/doi/10.1021/acs.chemrev.8b00361 (visited on 06/28/2025).

[32] *Density Functional Theory*, nl. [Online]. Available: https://www.tudelft.nl/tnw/over-faculteit/afdelingen/radiation-science-technology/research/research-groups/storage-of-electrochemical-energy/methods/density-functional-theory (visited on 06/30/2025).

[33] T. Dudev and C. Lim, "Tetrahedral vs Octahedral Zinc Complexes with Ligands of Biological Interest: A DFT/CDM Study," en, *Journal of the American Chemical Society*, vol. 122, no. 45, pp. 11 146–11 153, Nov. 2000, ISSN: 0002-7863, 1520-5126. DOI: 10.1021/ja0010296. [Online]. Available: https://pubs.acs.org/doi/10.1021/ja0010296 (visited on 05/15/2025).

[34] I. Y. Chernyshov and E. A. Pidko, "MACE: Automated Assessment of Stereochemistry of Transition Metal Complexes and Its Applications in Computational Catalysis," *Journal of Chemical Theory and Computation*, vol. 20, no. 5, pp. 2313–2320, Mar. 2024, ISSN: 1549-9618. DOI: 10.1021/acs.jctc.3c01313. [Online]. Available: https://doi.org/10.1021/acs.jctc.3c01313 (visited on 05/28/2025).

[35] Faccts, *ORCA*, en-GB. [Online]. Available: https://www.faccts.de/orca/ (visited on 06/28/2025).

[36] *Snellius: De Nationale Supercomputer — SURF.nl*, nl. [Online]. Available: https://www.surf.nl/diensten/rekenen/snellius-de-nationale-supercomputer (visited on 06/28/2025).

[37] M. S. Baidun, A. V. Kalikadien, L. Lefort, and E. A. Pidko, "Impact of Model Selection and Conformational Effects on the Descriptors for In Silico Screening Campaigns: A Case Study of Rh-Catalyzed Acrylate Hydrogenation," *The Journal of Physical Chemistry C*, vol. 128, no. 19, pp. 7987–7998, May 2024, ISSN: 1932-7447. DOI: 10.1021/acs.jpcc.4c01631. [Online]. Available: https://doi.org/10.1021/acs.jpcc.4c01631 (visited on 06/29/2025).

[38] *ORCA Forum - Portal*. [Online]. Available: https://orcaforum.kofo.mpg.de/app.php/portal (visited on 06/28/2025).

[39] *Infrared and Raman - ORCA 5.0 tutorials*. [Online]. Available: https://www.faccts.de/docs/orca/5.0/tutorials/spec/IR.html (visited on 05/30/2025).

[40] S. F. Sousa, P. A. Fernandes, and M. J. Ramos, "Comparative Assessment of Theoretical Methods for the Determination of Geometrical Properties in Biological Zinc Complexes," *The Journal of Physical Chemistry B*, vol. 111, no. 30, pp. 9146–9152, Aug. 2007, ISSN: 1520-6106. DOI: 10.1021/jp072538y. [Online]. Available: https://doi.org/10.1021/jp072538y (visited on 06/11/2025).

[41] *The Boltzmann distribution and the Gibbs free energy - Nexus Wiki*. [Online]. Available: https://www.compadre.org/nexusph/course/The_Boltzmann_distribution_and_the_Gibbs_free_energy (visited on 07/05/2025).

5 DECLARATION OF AI USE

In this project, the AI model ChatGPT was used as a helpful instrument to understand difficult terms or subjects. Additionally, it was used to assist with the code part of the writing editor LaTeX. When facing difficulties in Jupyter Notebook, ChatGPT was asked to rewrite python codes. Lastly, it was used to fix grammatical and structural issues in the text to improve clarity and fluency.